Biomaterials 35 (2014) 5731–5740

Contents lists available at ScienceDirect

Biomaterials

journal homepage: www.elsevier.com/locate/biomaterials

Multilevel surface engineering of nanostructured TiO_2 on carbon-fiber-reinforced polyetheretherketone

Tao Lu [a], Xuanyong Liu [a,*], Shi Qian [a], Huiliang Cao [a], Yuqin Qiao [a], Yongfeng Mei [b], Paul K. Chu [c], Chuanxian Ding [a]

[a] State Key Laboratory of High Performance Ceramics and Superfine Microstructure, Shanghai Institute of Ceramics, Chinese Academy of Sciences, Shanghai 200050, China
[b] Department of Materials Science, Fudan University, Shanghai 200433, China
[c] Department of Physics and Materials Science, City University of Hong Kong, Tat Chee Avenue, Kowloon, Hong Kong, China

ARTICLE INFO

Article history:
Received 30 January 2014
Accepted 1 April 2014
Available online 22 April 2014

Keywords:
Carbon-fiber-reinforced polyetheretherketone
Nanopores
Plasma immersion ion implantation
Osteogenic activity
Antibacterial activity

ABSTRACT

As an implantable material, carbon-fiber-reinforced polyetheretherketone (CFRPEEK) possesses an adjustable elastic modulus similar to that of cortical bone and is a prime candidate to replace metallic surgical implants. However, the bioinertness and poor osteogenic properties of CFRPEEK limit its clinical application as orthopedic implants. In this work, titanium ions are introduced energetically into CFRPEEK by plasma immersion ion implantation (PIII). Scanning electron microscopy (SEM) and X-ray photoelectron spectroscopy (XPS) reveal the formation of nanopores with the side wall and bottom embedded with ~20 nm TiO_2 nanoparticles on the CFRPEEK surface. Nanoindentation measurements confirm the stability and improved elastic resistance of the structured surfaces. *In vitro* cell adhesion, viability assay, and real-time PCR analyses disclose enhanced adhesion, proliferation, and osteo-differentiation of rat bone mesenchymal stem cells (bMSCs). The multilevel structures on CFRPEEK also exhibit partial antibacterial activity to *Staphylococcus aureus* and *Escherichia coli*. Our results indicate that a surface with multifunctional biological properties can be produced by multilevel surface engineering and application of CFRPEEK to orthopedic and dental implants can be broadened and expedited based on this scheme.

1. Introduction

Orthopedic implants are required when irreparable bone damage occurs due to trauma, disease, or congenital defects [1] and carbon-fiber-reinforced polyetheretherketone (CFRPEEK) is becoming a prime candidate to replace metallic implants [2,3]. Different from typical metallic materials which possess high elastic moduli of over 100 GPa, CFRPEEK has an adjustable elastic modulus close to that of cortical bone (18 GPa) which can mitigate concerns over the risks of osteanabrosis and bone resorption caused by stress shielding as a result of the elasticity mismatch between the implants and human bones [4,5]. In addition to its excellent mechanical properties, CFRPEEK inherits the non-toxicity, good chemical resistance, natural radiolucency, and even MRI (magnetic resonance imaging) compatibility from PEEK [2,3,6–8]. However, although the materials have attracted much attention as orthopedic implants since the 1980s, the bioinertness of CFRPEEK impedes osteointegration after implantation thereby severely hampering clinical adoption [2,3,9].

Surface modification is an effective way to enhance the surface mechanical and biological properties while the advantageous bulk properties of the materials can be preserved. Among the various surface modification techniques, plasma immersion ion implantation (PIII) is a non-line-of-sight method that has been widely applied to microelectronics, aerospace engineering, precision manufacturing, and biomedical engineering. By introducing different elements and functional groups, surface properties such as cytocompatibility, antibacterial activity, and mechanical properties can be selectively tailored [10–13]. Moreover, unique structures with different size can be formed selectively under proper conditions [14–16]. For example, pinnacle-like diamond-like carbon (DLC) coatings were by Wang et al. to reduce bacterial adhesion [14] and silver nanoparticles were formed on titanium and TiO_2 to enhance both the biocompatibility and antibacterial activities [15]. Recently, Qian et al. produced nanocap structures on TiO_2 nanotubes to alter the properties [16].

* Corresponding author. Fax: +86 21 52412409.
E-mail address: xyliu@mail.sic.ac.cn (X. Liu).

http://dx.doi.org/10.1016/j.biomaterials.2014.04.003
0142-9612/

It is well known that electrical micro-arcing induced by surface charging during PIII can cause surface damage to semi-insulating semiconductors and insulators [17–19]. However, unlike microelectronics, a "damaged" surface may be preferred in biomedical engineering because for instance, native bones possess a hierarchical structure on the micro-/nano-scale as well [20–23]. It has in fact been reported that some surface structures impact bacterial adhesion and growth [24,25]. TiO_2 nanotubes have attracted much attention because they can improve the adhesion and proliferation of osteoblasts and stem cells as well as up-regulate osteoblastic levels [22,26–28]. Besides, TiO_2 nanotubes provide an excellent platform for drug delivery for growth factors and antibacterial agents [29,30]. However, there have been few studies concerning TiO_2 nanotube coatings on polymers due to the practical limitation of anodic oxidation.

In this work, TiO_2 nanotube-like multilevel structures are produced on CFRPEEK by titanium plasma immersion ion implantation (Ti-PIII). Micro-arcing occurring during high frequency, long pulse, and long implantation time PIII produces special nanopores with TiO_2 walls on the CFRPEEK surface. The osteogenic properties of the structured CFRPEEK surface are evaluated using rat bMSCs and the antibacterial activity against *Staphylococcus aureus* and *Escherichia coli* is assessed *in vitro*. A model is proposed to discuss the formation mechanism of the multilevel structure.

2. Materials and methods

2.1. Sample preparation

Biomedical grade carbon-fiber-reinforced polyetheretherketone (CFRPEEK) with 30% (v/v) carbon fibers was used in this study. The samples were machined into different dimensions. Square samples ($10 \times 10 \times 1$ mm^3) were used for surface characterization, immersion tests, and *in vitro* studies on 24-well tissue culture plates. Square samples with a different size ($20 \times 20 \times 1$ mm^3) were used in the real-time PCR tests. All the samples were polished on one side to a near mirror finish and ultrasonically cleaned in acetone, ethanol, and ultra-pure water prior to PIII. Titanium ions were implanted into the CFRPEEK samples using a filtered cathodic arc source housing a 99.99% pure titanium rod with a diameter of 10 mm. Before PIII, the chamber was evacuated to a pressure of 5×10^{-3} Pa. By applying a pulsed negative high voltage to CFRPEEK sample on the sample stage, Ti ions were implanted and the sample stage was continuously rotated during PIII to obtain uniform ion implantation. Table 1 lists the important parameters and sample designation. The sample after undergoing Ti-PIII at 30 kV for 120 min is designated as Ti-120.

2.2. Surface structure and chemical characterization

The surface and cross-section of the CFRPEEK samples were examined by field-emission scanning electron microscopy (FE-SEM, Hitachi S-4800, Japan) at different magnification without applying a conductive coating. The surface chemical states and elemental depth profiles were determined by X-ray photoelectron spectroscopy (XPS, Physical Electronic PHI 5802 equipped with a monochromatic Al K_α source) in City University of Hong Kong. The C, O, and Ti profiles were acquired by XPS in conjunction with argon ion bombardment at a sputtering rate of about 4 nm/min. Nanoindentation was performed at loadings of 1.3 mN and 3.0 mN and the results of at least eight indents were averaged to improve the statistics.

2.3. Ion release

Two pieces of each sample were incubated in 5 mL of phosphate buffered saline (PBS 1 M) for different immersion time (7, 14, 21, and 28 days) at 37 °C without stirring. At a prescribed time, the solution was withdrawn and analyzed by inductively-coupled plasma atomic emission spectroscopy (ICP-AES, JY 2000-2, France) analysis to determine the amount of released titanium.

Table 1
Main conditions in titanium plasma immersion ion implantation of Ti-120.

Parameters	Description
Cathode source	99.99% pure Ti
Voltage pulse duration (μs)	500
Pulsing frequency (Hz)	7
Ion implantation voltage (kV)	−30
Ion implantation time (min)	120
Pressure (Pa)	5×10^{-3}

Table 2
Primer pairs used in real-time PCR analysis.

Gene	Primers (F = forward, R = reverse)	Amplicon
COL-I	F: CTGCCCAGAAGAATATGTATCACC R: GAAGCAAAGTTTCCTCCAAGACC	198 bp
Runx2	F: TCTTCCCAAAGCCAGAGCG R: TGCCATTCGAGGTGGTCG	154 bp
BMP-2	F: TGGGTTTGTGGTGGAAGTGGC R: TGGATGTCCTTTACCGTCGTG	154 bp
ALP	F: CGTCTCCATGGTGGATTATGCT R: CCCAGGCACAGTGGTCAAG	209 bp
OCN	F: GCCCTGACTGCATTCTGCCTCT R: TCACCACCTTACTGCCCTCCTG	103 bp
OPN	F: CCAAGCGTGGAAACACACAGCC R: GGCTTTGGAACTCGCCTGACTG	165 bp
β-actin	F: CACCCGCGAGTACAACCTTC R: CCCATACCCACCATCACACC	207 bp

2.4. Cell culture

The bone mesenchymal stem cells (bMSCs acquired from Cells Resource Center, Shanghai Institutes of Biological Science, Shanghai, China) were isolated from the bone marrow of six-week-old male Fisher 344 rats. The bMSCs were cultured in the α-minimum essential medium (α-MEM, Gibto-BRL, USA) with 10% fetal bovine serum (FBS, Hyclone, USA), 1% antimicrobial of penicillin, and streptomycin at 37 °C in a humidified atmosphere of 5% CO_2. The α-MEM was refreshed every 3 days during cell culturing. The experiments were carried out with the bMSCs before passage five. All the samples were sterilized with 75% alcohol for 3 h and rinsed twice with sterile PBS before cell seeding.

2.5. Cell adhesion

The bMSCs were seeded on the samples on a 24-well plate at the density of 5×10^4 cells per well. After 1, 3, and 24 h, the samples were taken to another 24-well plate. The samples were rinsed twice with PBS and fixed with 3% glutaraldehyde overnight. Ethanol with different concentrations of 30, 50, 75, 90, 95, 100, and 100% v/v was used sequentially to dehydrate the samples for 10 min. The samples were finally dehydrated in a series of hexamethyldisilizane (HMDS) ethanol solution and the dried samples were sputter coated with platinum for SEM (Hitachi S-3400, Japan) observation.

2.6. Cell proliferation and viability

The alamarBlue™ (AbD Serotec Ltd, UK) assay was employed to quantitatively determine the cell proliferation and viability on the samples. The bMSCs were seeded on the samples (four replicates) on 24-well plates at the density of 2.5×10^4 cells per well. After 1, 4 and 7 days, the culture medium was replaced by 0.5 mL of the fresh medium with 5% alamarBlue™ in each well. After incubation for 4 h, 100 μL of the medium was transferred to a 96-well plate for measurement. The amount of reduced alamarBlue™ was determined by an enzyme-labeling instrument (BIO-TEK, ELX 800) at wavelengths of 570 nm and 600 nm. The operation and calculation of cell proliferation followed the instruction of the alamarBlue™ assay.

2.7. Alkaline phosphatase activity

The bMSCs were seeded on the samples (four replicates) on 24-well plates at a density of 1×10^4 cells per well (cultured for 7 days) or 0.5×10^4 cells per well (cultured for 14 days). In the quantitative alkaline phosphatase (*ALP*) assay, after culturing for 7 and 14 days, a Bio-Rad protein assay kit (Bio-Rad, USA) was used to calculate the total protein content and the results were adjusted with a series of BSA (Sigma) standards by measuring the optical density (OD) values of the absorbance at 570 nm. After incubation with p-nitrophenyl phosphate (Sigma) at 37 °C for 30 min, the *ALP* activity was calculated and adjusted with a series of 4-Nitrophend NaOH (0.02 M) solutions by measuring the OD values at 405 nm. The *ALP* levels were normalized to the total protein content and described as μM/mg total proteins.

2.8. Quantitative real-time PCR

The expression of osteogenesis-related genes was analyzed using quantitative real-time reverse-transcriptase polymerase chain reaction (real-time PCR). Three pieces of each sample were placed on the cell culture dish (6 cm diameter, Nunc, Denmark). The bMSCs were seeded on the dish at a density of 1×10^5 cells per dish (cultured for 7 days) or 0.5×10^5 cells per dish (cultured for 14 days). The total RNA was extracted using TRIZOL reagent (Invitrogen, USA) and the complementary DNA (cDNA) was reverse-transcribed from 1 μg of total RNA using a PrimeScript I Strand cDNA Synthesis kit (TaKaRa) according to the manufacturer's protocols. The forward and reverse primers for different genes are listed in Table 2. The expression of selected genes, including Type I collagen (*COL-I*), runt-related transcription factor 2 (*Runx2*), bone morphogenetic protein 2 (*BMP-2*), alkaline phosphatase (*ALP*),

osteocalcin (*OCN*), and osteopontin (*OPN*) were analyzed with *β-actin* as the housekeeping gene for normalization and relatively quantified using real-time PCR (LightCycler 480 Real-Time PCR System, Roche, USA) using the following procedures: denaturation at 95 °C for 30 s and 40 cycles of PCR (95 °C for 10 s and 60 °C for 20 s). Quantification of gene expression was based on the CT (cycle threshold) values.

2.9. Antibacterial tests

The antibacterial activity was assessed by the bacterial counting method using *Staphylococcus aureus* (*S. aureus*, ATCC 25923) and *Escherichia coli* (*E. coli*, ATCC 25922). *S. aureus* was cultured on the tryptic soy broth or agar (TSB) plates and *E. coli* was cultured on Luria-bertani or agar (LB) plates. All samples were sterilized with 75% alcohol for 3 h and rinsed twice with sterile PBS before bacteria seeding. A 60 μL suspension with a concentration of 10^7 cfu/mL bacteria was dropped onto the samples. After culturing for 24 h at 37 °C, the samples with the suspension were put into each sterilized centrifugal tube with 5 mL of 0.9% physiological saline. The tube was vigorously agitated for 30 s to detach the bacteria form the sample surface. Subsequently, the detached bacteria suspension was diluted 10, 100, and 1000 times. 150 μL of the diluted bacteria suspension was introduced onto the TSB or LB plates. After culturing for 24 h at 37 °C, the active bacteria were counted according to the National Standard of China GB/T 4789.2 protocol. The morphology of the bacteria was examined by SEM. The samples were placed in 60 μL of the suspension at a bacteria concentration of 10^7 cfu/mL and cultured for 24 h at 37 °C. At the end of culturing, the samples were rinsed twice with PBS and fixed with 3% glutaraldehyde overnight. A series of ethanol solutions (30, 50, 75, 90, 95, 100 and 100% v/v) was used to dehydrate the samples for 10 min sequentially. The samples were finally dehydrated in a series of hexamethyldisilizane (HMDS) ethanol solution and the dried samples were sputter coated with platinum prior to SEM observation.

2.10. Statistical analysis

Statistically significant differences (p) between groups were measured using the one-way analysis of the variance and Tukey's multiple comparison tests. All the statistical analyses were determined with the GraphPad Prism 5 statistical software package.

3. Results

3.1. Characterization of surface

The surface of the CFRPEEK samples before and after Ti-PIII is shown in Fig. 1. The untreated CFRPEEK (Fig. 1A and B) has a relatively flat and smooth surface due to pre-polishing but disordered carbon fibers can be clearly seen from the CFRPEEK surface. After Ti-PIII, nanopores emerge from the area without carbon fibers on Ti-120, as shown in Fig. 1C and D. Most of the nanopores with diameters between 150 and 200 nm are distributed homogeneously on the surface of CFRPEEK, while others have incomplete side structures and blend with each other. The higher magnification view reveals a secondary structure consisting of nanoparticles on the sidewall and bottom of the nanopores (insert in Fig. 1D). The nanoparticles formed on Ti-120 during PIII have estimated size of 20 nm.

Fig. 2 displays the cross-sectional images of CFRPEEK and Ti-120. No obvious structures can be observed from the outer surface before Ti-PIII. A modified layer with a thickness of about 800 nm appears on Ti-120 and there are apparent tunnels penetrating the entire modified layer. The high-magnification images of Ti-120 confirm that the nanoparticles fully cover the inside walls of the nanopores. As is shown in Fig. 2C and D, the nanoporous structure has an inverted conical shape (marked by the white lines in Fig. 2D) and the diameter of the nanopores decreases gradually along the direction to the substrate.

The elemental chemical states of the sample surface are shown in Fig. 3. In comparison with the XPS full spectra of CFRPEEK (Fig. 3A), the characteristic peaks of Ti are detected from Ti-120 (Fig. 3B). A clean XPS full spectrum is acquired from Ti-120 and no other elements are detected. The high-resolution spectra indicate that the Ti 2p peaks are at 459.01 eV and 464.73 eV and O 1s peaks are at 530.50 eV and 531.50 eV (Fig. 3C and D), corresponding to the typical binding energy of TiO_2 [31,32]. The C, O and Ti depth profiles are depicted in Fig. 3E. The absolute concentrations are only approximate due to indirect calibration and the existence of nanostructure, but profile-to-profile comparison is reliable. The ratio of O to Ti in the near surface is close to 2:1, providing evidence that the nanoparticles are stoichiometric TiO_2. The ratio of O to Ti decreases with depth indicating the existence of possible oxygen vacancies in the nanoparticles. The Ti concentration is about 31 at.% at a depth of 5 nm and Ti can be detected up to 400 nm which is deeper than that reported earlier. Hence, PIII can produce a continuous Ti-doped layer without an abrupt interface to a reasonable depth.

The load-displacement curves of CFRPEEK and Ti-120 samples are shown in Fig. 4. Continuous curves are observed during the loading

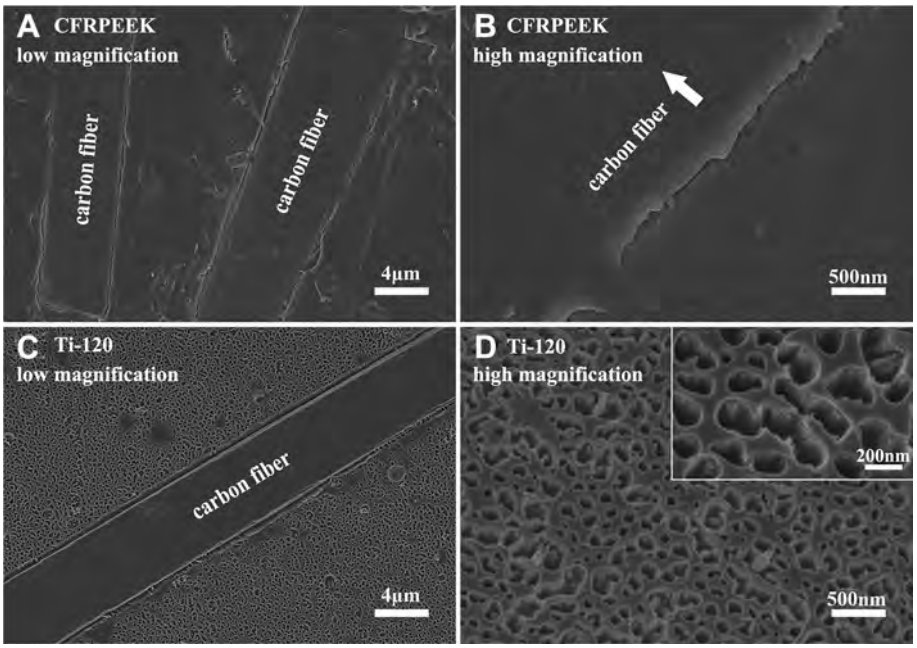

Fig. 1. Surface views of CFRPEEK and Ti-120 samples: (A) CFRPEEK at low magnification (×5000); (B) CFRPEEK at high magnification (×50000); (C) Ti-120 at low magnification (×5000); (D) Ti-120 at high magnification (×50000). The insert on top right corner in (D) is high magnification of Ti-120 (×100000). The carbon fiber is marked by white arrow in (B).

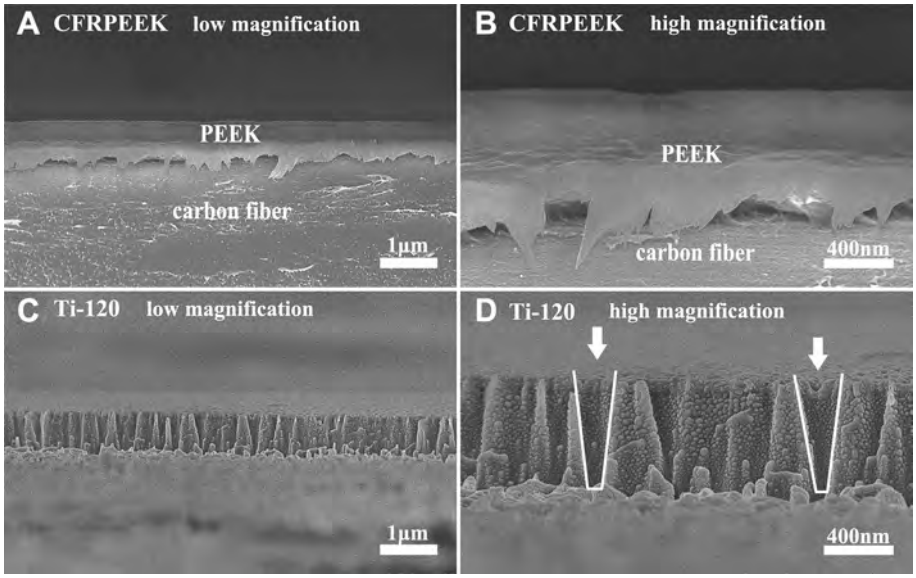

Fig. 2. Cross-sectional morphology of CFRPEEK and Ti-120 samples: (A) CFRPEEK at low magnification (×10000); (B) CFRPEEK at high magnification (×30000); (C) Ti-120 at low magnification (×10000); (D) Ti-120 at high magnification (×30000).

and unloading stages of Ti-120, indicating that no abrupt cracking of the nanoporous layer occurs during the whole process. At the same load, the indentation depth of Ti-120 is smaller and the elastic recovery of Ti-120 is larger than that of CFRPEEK, suggesting a higher elastic resistance due to the existence of nanopores after Ti-PIII.

3.2. Response of bMSCs

The bMSC cells exist abundantly in bone marrow and are considered ideal cells for the evaluation of cytocompatibility and osteogenic properties of bone substitutes. The initial adhesion behavior of bMSCs on CFRPEEK and Ti-120 after 1, 3, and 24 h is monitored by SEM as shown in Fig. 5. The bMSCs on the CFRPEEK surface exhibit a round morphology in the first hour but those on Ti-120 surface show more filopodia and lamellipodia extensions. After 24 h, the cells adhere well onto both surfaces with the typical morphology, although the cells on Ti-120 are more elongated, indicating that the nanopores alter the initial cellular adherence.

The time-related proliferation of bMSCs cultured on both samples is evaluated by the alamarblue™ assay and the data are presented in Fig. 6. Cell proliferation on Ti-120 is statistically higher ($p < 0.05$) than that on CFRPEEK after 1 day. This is consistent with

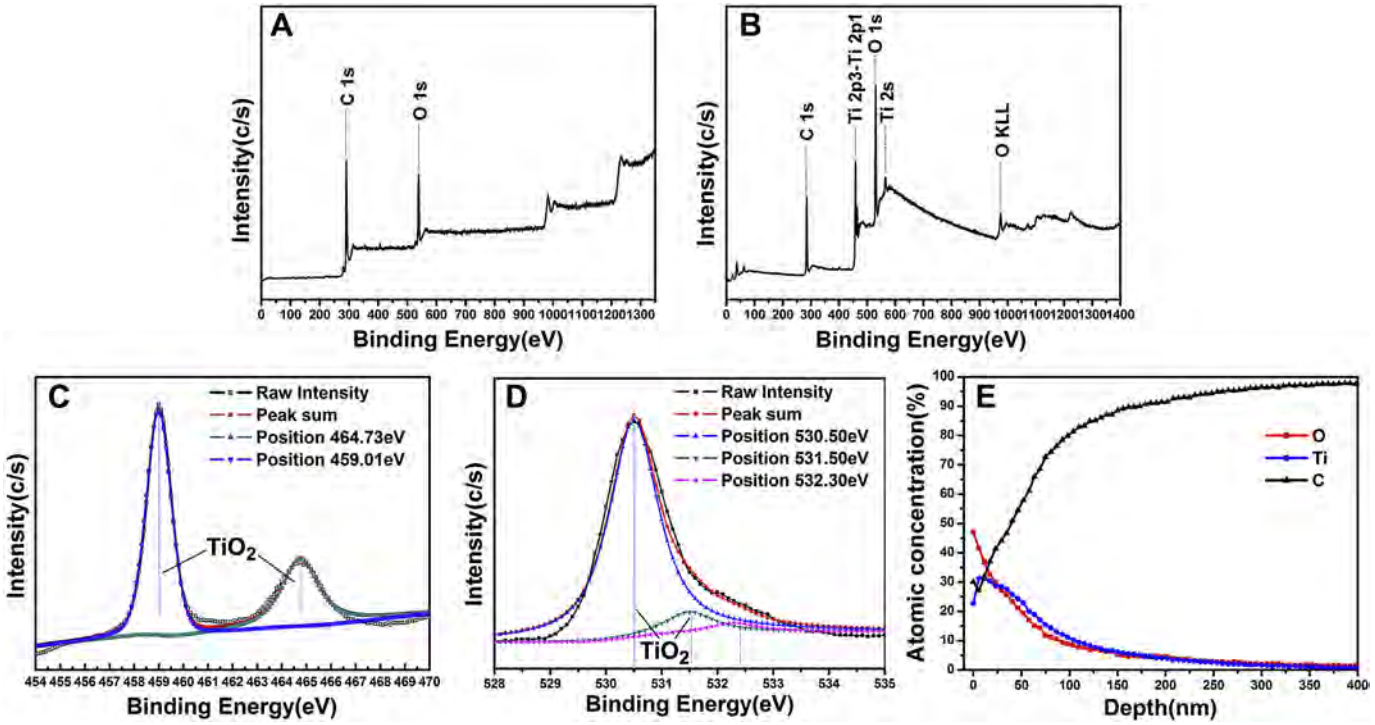

Fig. 3. XPS spectra: (A) XPS full spectra from CFRPEEK; (B) XPS full spectra from Ti-120; (C) Ti 2p XPS spectra from Ti-120; (D) O 1s XPS spectra from Ti-120; (E) C, O and Ti depth profiles obtained from Ti-120.

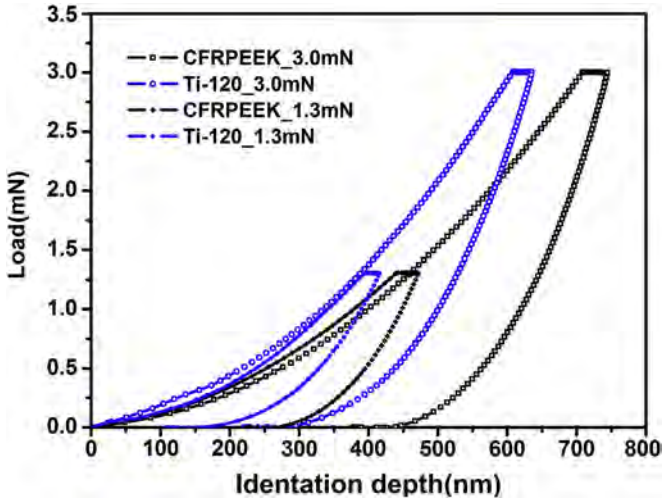

Fig. 4. Load-displacement curves of CFRPEEK and Ti-120 samples at indentation loads of 1.3 mN and 3.0 mN.

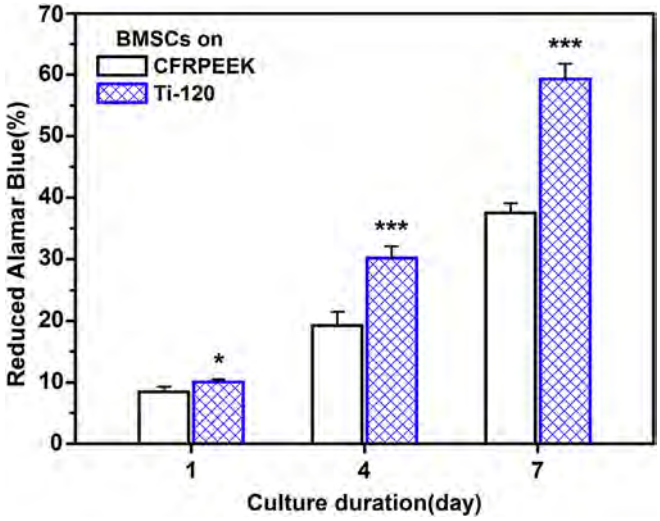

Fig. 6. Reduction percentage of alamarBlue™ for bMSCs cultured on CFRPEEK and Ti-120 for 1, 4 and 7 days and the statistical significance indicated by *($p < 0.05$), ***($p < 0.001$).

the adherence results of bMSCs for 24 h. Furthermore, as the culturing time is increased to 4 and 7 days, the number of cells on Ti-120 continues to be larger and the difference becomes bigger ($p < 0.001$), indicating that Ti-120 is more favorable to bMSC proliferation and the nanoparticles on Ti-120 induce no apparent toxicity to the bMSCs.

The osteoblastic differentiation ability of bMSCs is critical to bone regeneration and alkaline phosphatase (*ALP*) is an early marker of osteogenic differentiation. In this study, the *ALP* expression on Ti-120 is significantly ($p < 0.001$) up-regulated after culturing for 7 and 14 days (Fig. 7), demonstrating the stimulating effects of the nanopores on bMSCs osteo-differentiation.

Fig. 8 displays the osteogenic differentiation properties assessed by quantitative real-time PCR of typical osteogenesis-related gene expression for 7 and 14 days, including *COL-I*, *Runx2*, *BMP-2*, *ALP*, *OCN*, and *OPN*. The difference in the gene expression between CFRPEEK and Ti-120 increases with time extends. At two time points, the bMSCs on Ti-120 show higher ($p < 0.001$) mRNA expression of *COL-I*, *BMP-2*, *ALP*, *OCN*, and *OPN* than CFRPEEK after 7 and 14 days, although the *Runx2* expression shows no difference statistically. *COL-I* is one of the major components in the extra cellular matrix and accounts for 90% of the protein mass in the organic part of bone. *BMP-2* is one of bone morphogenetic proteins and has been demonstrated to induce osteoblastic differentiation. The higher expression of *COL-I* and *BMP-2* indicates that osteoblastic differentiation happens ubiquitously and more actively on Ti-120. In particular, as the culturing time is prolonged to 14 days, the *OCN* (a calcium binding protein, marker for the bone formation process and playing an important role in bone-building) and *OPN* (a phoshoprotein playing a crucial role in anchoring osteoclasts to the mineral matrix of bones) expression between the two surfaces becomes more significant (16 and 6 times higher, respectively), indicating the osteoblastic differentiation is accelerated on Ti-120.

3.3. Antibacterial activity

Antibacterial activity is one of the main factors that influence the interactions between the biomedical implants and human body. In this work, the bacteria (*S. aureus* and *E. coli*) counting method is used to evaluate the bactericidal effects of Ti-120. The bacteria colony photos are shown in Fig. 9. The amount of *S. aureus* on Ti-120 is reduced by 71.4 ± 3.5% after 24 h whereas that of *E. coli* shows no significant difference (reduced by 5.3 ± 1.3%).

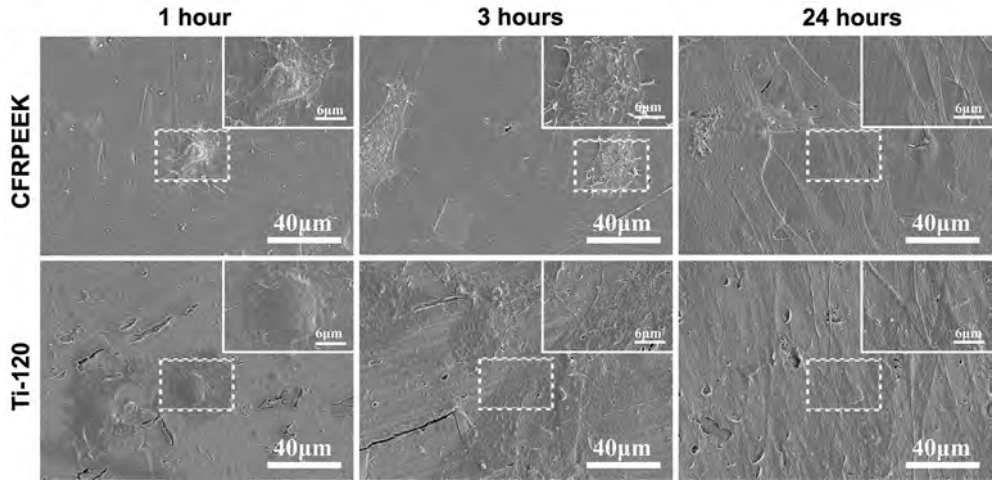

Fig. 5. SEM morphology of the bMSCs adhered on CFRPEEK and Ti-120 after 1, 3, and 24 h. The insert on top right corner is high magnification of dash line marked area, respectively.

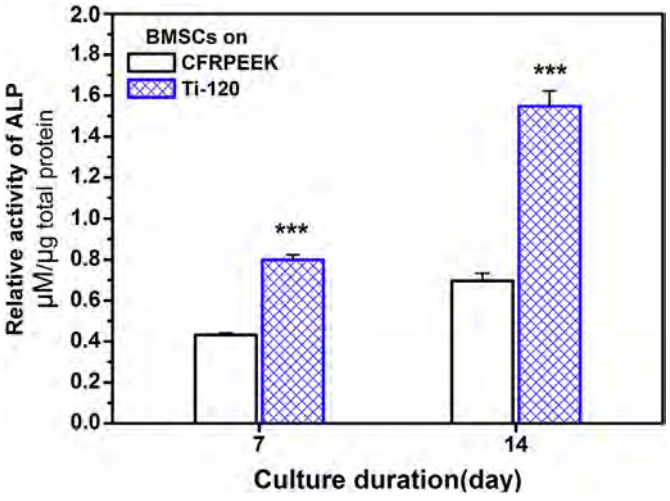

Fig. 7. *ALP* activity assay of the bMSCs cultured on CFRPEEK and Ti-120 for 7 and 14 days with the statistical significance indicated by ***($p < 0.001$).

The morphology of the bacteria is examined by SEM (Fig. 10). The *S. aureus* bacteria on CFRPEEK accumulate to a typical shape of staphylococcus (Fig. 10A) and display an intact surface whereas on Ti-120, *S. aureus* bacteria prefer to accumulate on the carbon fibers (Fig. 10B), indicating the nanostructures contribute mostly to the *S. aureus* bacteria reduction. Some *S. aureus* bacteria attached to the area covered by the nanopores have a rough surface and debris of lysed cells can be found on Ti-120 as well (marked by black arrows, Fig. 10C). With regard to *E. coli*, although there is no obvious quantitative difference statistically between the two samples (Fig. 10D and E), the *E. coli* cells observed on Ti-120 (Fig. 10F) have an irregular cell shape (marked by white arrows) and shriveled cell surface (marked by black arrows), indicating that abnormal metabolism happens to the *E. coli* cells.

4. Discussion

Plasma immersion ion implantation (PIII) is an effective way to change selective surface properties. By immersing the samples in a plasma and applying a negative voltage pulses, the sample is implanted conformally under optimal conditions thus boding well for treatment of orthopedic implants with a complex geometry. Previous studies have mainly focused on the alteration of surface chemistry due to introduction of new implanted elements or functional groups but not much attention has been paid to structural variations under complicated thermal and physical conditions [33–39]. In the present work, plasma immersion ion implantation technique is conducted on CFRPEEK and nanopores with TiO_2 walls are observed to form on the surface. A model in which thermal ablation and dielectric breakdown are considered as the driving force of the nanostructure formation is proposed. In this model, the nanostructure is formed in two stages. The first one involves thermal coarsening. During PIII using a cathodic arc, ions gain kinetic energy including E_0 near the cathode spot, QeV_{sheath} (charge state is Q, e is the elementary charge, and V_{sheath} is the plasma sheath voltage) when ions pass through the plasma sheath, and E_{ic} induced by image charge acceleration. The potential energy includes excitation energy E_{exc}, cohesive energy E_c, and ionization energy. The general expression of the total energy of an incident ion is described by Equation (1) [40]:

$$E_t = E_0 + QeV_{\text{sheath}} + E_{\text{ic}} + E_c + E_{\text{exc}} + \sum_{i=0}^{Q-1} E_i. \quad (1)$$

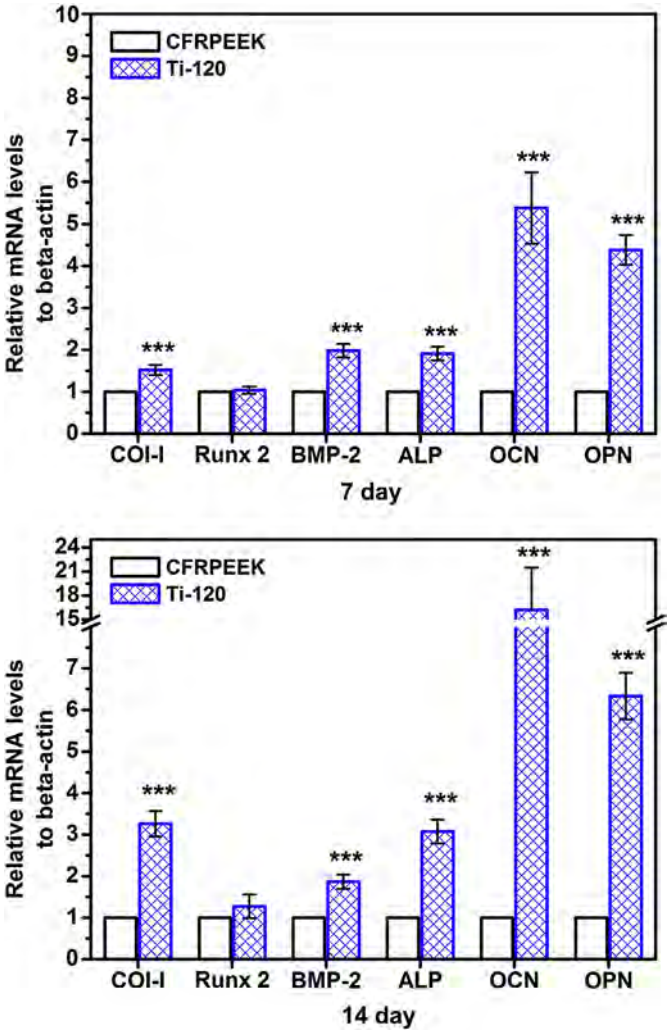

Fig. 8. Real-time PCR detection of osteogenesis-related gene expression of the bMSCs cultured on CFRPEEK and Ti-120 for 7 and 14 days with the statistical significance indicated by ***($p < 0.001$).

When ions penetrate the sample surface before stopping, some of the total energy is converted into thermal energy *via* atomic scale heating (ASH) [40]. At a high voltage (V_{sheath}), the ions obtain most of the energy when passing through the plasma sheath and hence, ASH depends mainly on Q and V_{sheath}. Sometimes ASH can be quite large due to the poor thermal conductivity of the substrate. In our experiments, CFRPEEK is implanted with high-energy Ti ions (listed in Table 3). In the early stage, titanium atoms are distributed homogeneously on the surface forming small conductors. In the meantime, non-equilibrium heat generated by ASH accumulates on the surface and is preferentially concentrated at the titanium conductor to initiate thermal ablation of the polymeric substrate forming small nanopits on the surface as shown in Fig. 11 (Stage I and Stage II) and Fig. 12. The growth of titanium nanoparticles evolves from small titanium conductors due to the thermal concentration.

The second stage is dielectric breakdown. As ion implantation proceeds, the titanium layer formed on the surface constitutes a typical plate capacitor in the presence of carbon fibers. Besides, owing to the poor thermal conductivity of the polymer substrate, ASH ablates the surface creating numerous nanopits, while thermal diffusion causes deeper penetration of Ti as aforementioned acting as defects in the conductive plate. This occurs in concert with

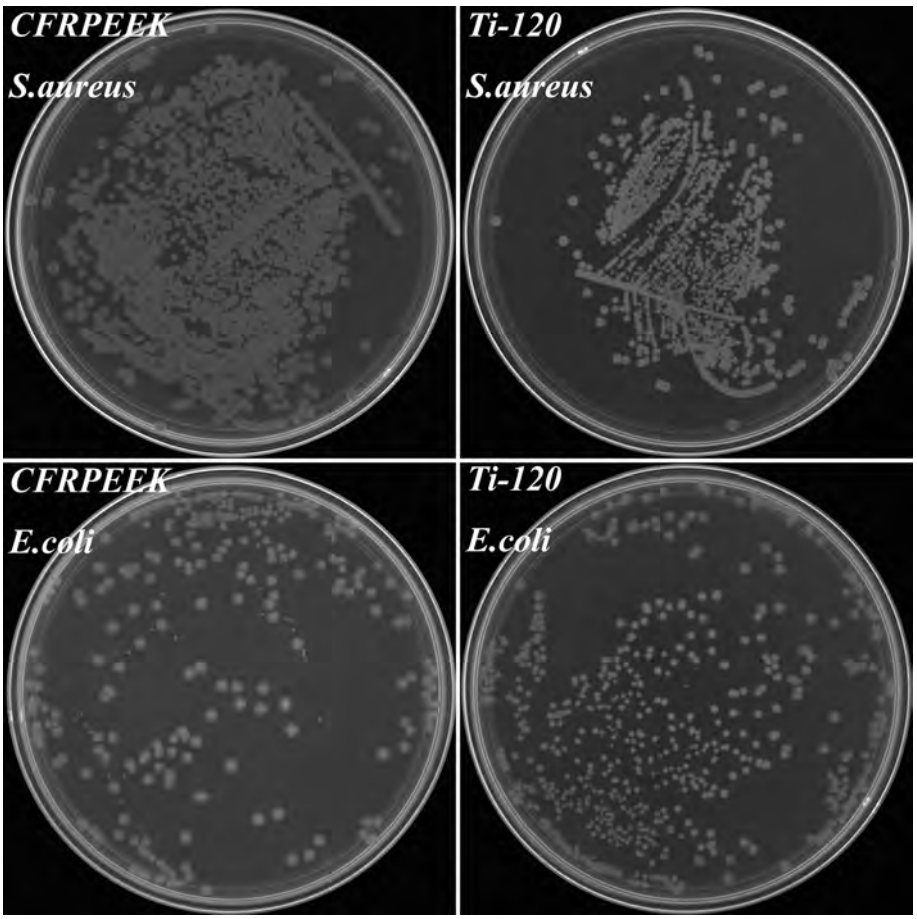

Fig. 9. Re-cultivated bacterial colonies on agar: *S. aureus* and *E. coli* colonies are previously dissociated from CFRPEEK and Ti-120. The *S. aureus* and *E. coli* bacteria concentration seeded on the samples is 10^7 cfu/mL.

sample charging which occurs during PIII, as illustrated in Fig. 11 as Stage I and Stage II. It is known that defects in the substrate will lead to a concentrated field, under which avalanche multiplication arises leading to dielectric breakdown. In this case, the relative depth of the incident Ti atom is described as a, which is much less than the sample thickness d ($d >> a$). Therefore, Ti atoms in the deeper region can be regarded as point electrodes which can initiate dielectric breakdown as soon as the electric field (E_{bd})

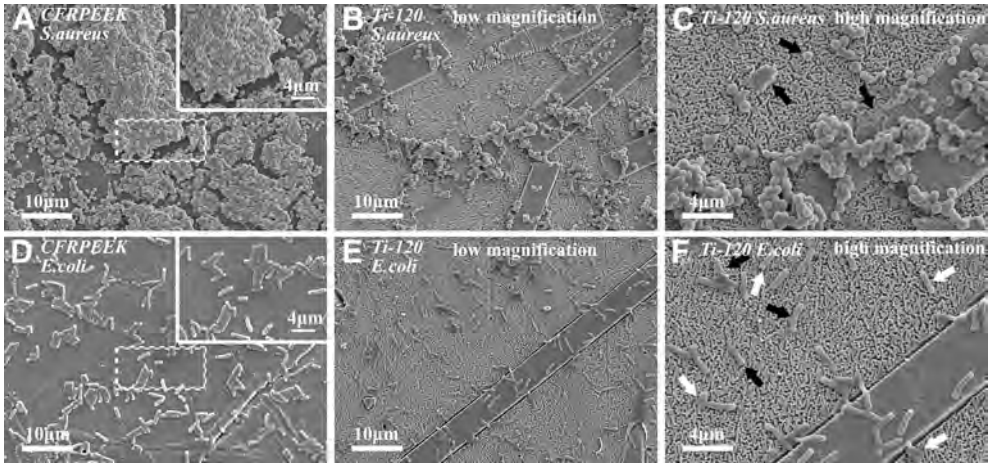

Fig. 10. SEM morphology of bacteria on samples: (A) *S. aureus* on CFRPEEK; (B) *S. aureus* on Ti-120 at low magnification; (C) *S. aureus* on Ti-120 at high magnification; (D) *E.coli* on CFRPEEK; (E) *E.coli* on Ti-120 at low magnification; (F) *E.coli* on Ti-120 at high magnification. The *S. aureus* and *E. coli* concentration seeded on the samples is 10^7 cfu/mL. The insert on top right corner in (A) and (B) is high magnification of dash line marked area, respectively. Debris of lysed bacterial cells is marked by black arrows and bacterial cells with irregular shape are marked by white arrows.

Table 3
Main conditions in titanium plasma immersion ion implantation.

Substrates	Cathode sources	Voltage [-kV]	Treatment time [min]	Sample names
PEEK	–	–	–	PEEK
PEEK	Ti	30	120	Ti-PEEK
CFRPEEK	Ti	30	60	Ti-60
CFRPEEK	Ti	30	90	Ti-90

exceeds 190 kV/mm, the intrinsic breakdown field strength of PEEK provided by the manufacturer. This leads to point discharge and formation of the inverted conical nanopores as shown in Fig. 11 as Stage III and Stage IV [41]. The minimum depth of Ti, a_{min}, can be calculated according to Equation (2) [41]:

$$a_{min} = \frac{3}{16} d \left(\frac{E_{bd}}{E_c} \right)^2 . \quad (2)$$

Although the exact critical electric field E_c near the filament is difficult to determine, it can be estimated according to the experiments of Hibma and Zeller [42]. They measured a critical electric field of 1600 kV/mm with gold needle tips with a radius of 1 μm in epoxy resin. Based on E_{bd} = 190 kV/mm at d = 1 mm, it can be

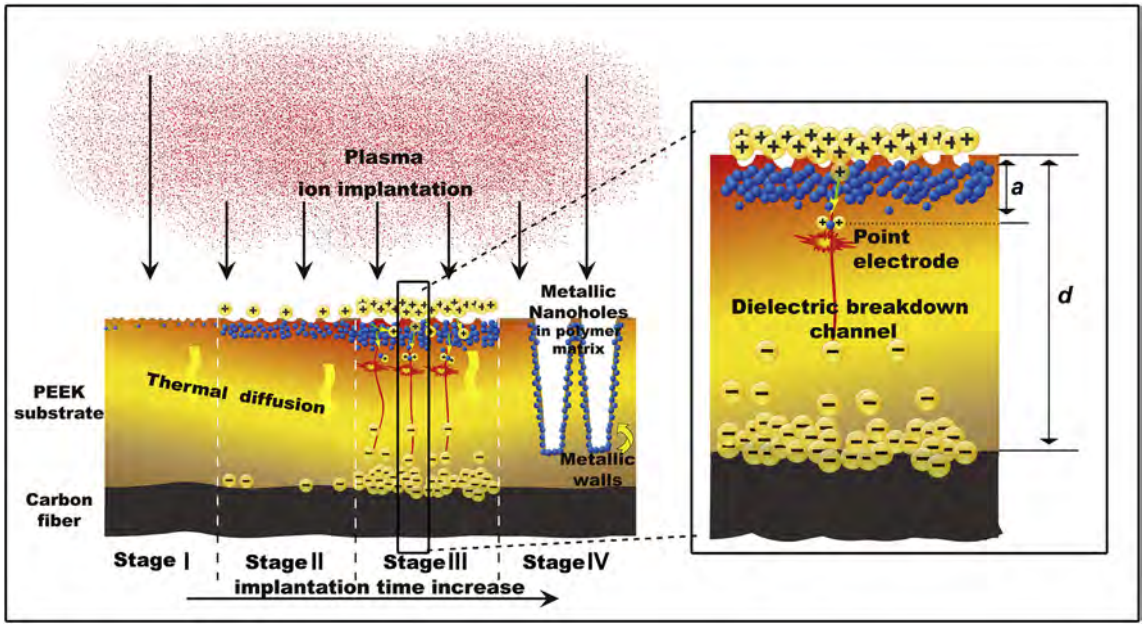

Fig. 11. Schematic illustration of the formation mechanism of nanopores with TiO_2 walls.

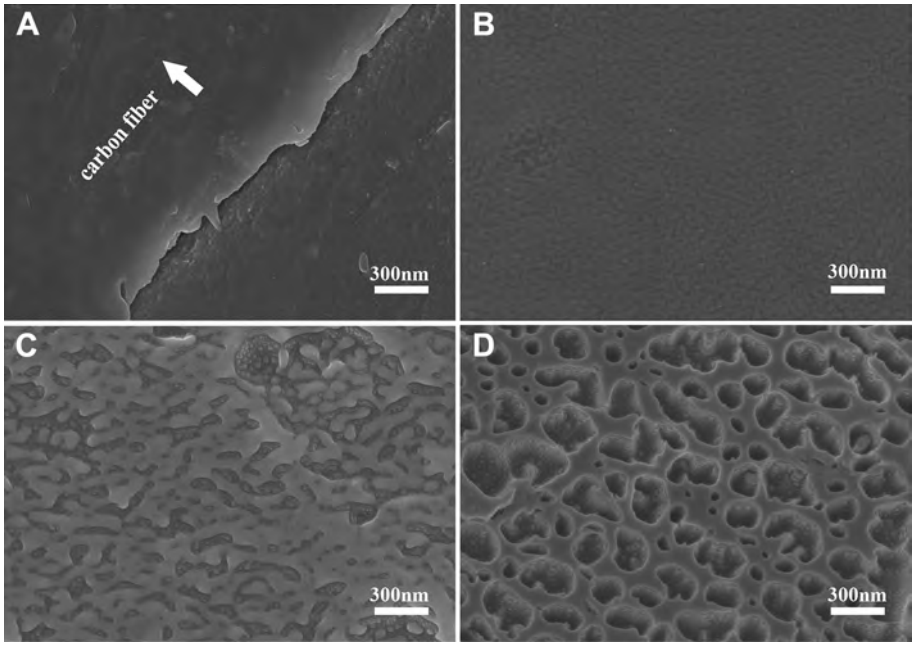

Fig. 12. Surface morphology of CFRPEEK after Ti-PIII for different time: (A) 0 min (CFRPEEK); (B) 60 min (Ti-60); (C) 90 min (Ti-90); (D) 120 min (Ti-120). The carbon fiber is marked by white arrow in (A).

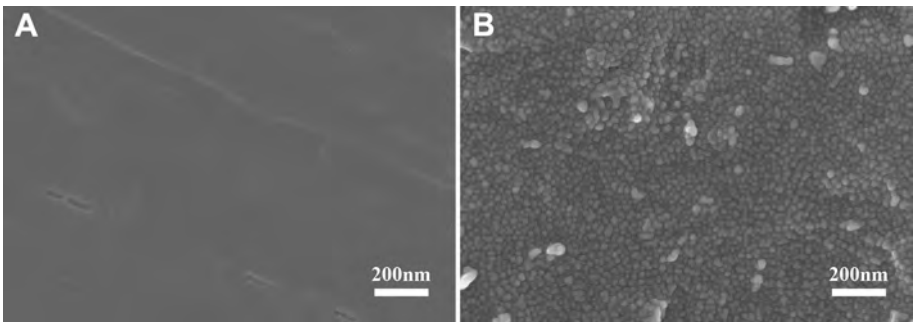

Fig. 13. Surface morphology of PEEK and Ti-PEEK: (A) PEEK and (B) Ti-PEEK.

estimated that $a_{min} \approx 2600$ nm in pure PEEK, which is hardly achievable by PIII (Fig. 13). In the presence of carbon fibers in the near surface, the plate capacitor thickness d is largely reduced. Under the same conditions when d is reduced to 50 μm, it can be estimated that the minimum depth $a_{min} \approx 130$ nm is achievable by Ti-PIII. To corroborate our hypothesis, CFRPEEK is subjected to other metal-PIII processes such as Zn-PIII and Zr-PIII, and nanopores are also produced on the surface (data not shown). Therefore, nanopore formation is not specific to Ti-PIII and by adopting the appropriate conditions, nanopores of various morphologies can be fabricated by conducting metal-PIII on CFRPEEK or other polymeric substrates.

As discussed above, ion doping as well as structure fabrication are simultaneously achieved on CFRPEEK by Ti-PIII. As confirmed by SEM and XPS (Figs. 1–3), special nanopores with TiO_2 walls similar to TiO_2 nanotubes appear. This structure acquired by Ti-PIII is a top-down structure, corresponding to decreased concentration of Ti with depth (Fig. 3E). Therefore, there is no distinct boundary between the structured layer and substrate and so abrupt delamination which usually occurs in samples with discrete interfaces does not occur in our samples. As a result, there is better adhesion between the modified layer and substrate.

One of the reasons to substitute Ti alloys with biopolymers such as PEEK and CFRPEEK is that the polymers have an elastic modulus similar to that of cortical bones. However, the elastic modulus of biopolymers still needs to be adjusted [4]. Hence, in addition to the surface morphology, the surface mechanical properties and stability must be examined to ensure sufficient safety *in vivo*. In PIII, dehydrogenation, crosslinking, and atom supersaturation occurring in the near surface can enhance the surface mechanical properties of polymers [43]. In this work, the CFRPEEK surface is bombarded by Ti ions for 120 min and the elastic modulus is improved. In fact, formation of the multilevel structures does not occur at the expense of mechanical properties and stability, as corroborated by the better elastic resistance of Ti-120 shown in Fig. 4.

TiO_2 nanotubes prepared on titanium have been extensively investigated and TiO_2 nanotube coatings have been shown to alter the cell behavior such as adhesion, proliferation, as well as differentiation of bone mesenchymal stem cells (bMSCs) [44,45]. It is generally believed that TiO_2 nanotubes with a small diameter is favorable to integrin clustering and consequently better cell adhesion and proliferation, whereas TiO_2 nanotubes with a large diameter produce an elongated cellular morphology and direct bMSCs to osteo-differentiation [27,28]. Antibacterial studies show that TiO_2 nanotubes can increase bacteria killing on contact [25]. The most likely cause of bacteria death is the reactive oxygen species generated from oxygen vacancies in anodized TiO_2 nanotubes. Here, as inferred from the morphology and XPS data, the nanopores with TiO_2 wall in CFRPEEK may possess effects similar to those of conventional TiO_2 nanotubes, and biological experiments are conducted to evaluate the characteristics.

According to our results, after the nanopores with TiO_2 walls are fabricated on the surface, adhesion (Fig. 5), proliferation (Fig. 6), and osteoblastic differentiation (Figs. 7 and 8) of bMSCs are all improved. We believe that the special multilayered structure activates cell responses at different levels. Park et al. found that TiO_2 nanotubes with a diameter of 15 nm–30 nm were favorable to integrin clustering consequently lead to better cell adhesion and proliferation, whereas TiO_2 nanotubes with a large diameter could produce an elongated cellular morphology and direct bMSCs to osteo-differentiation [27,28]. Here, a combined structure with different size is acquired. TiO_2 nanoparticles are considered to play a key role in cell adherence. The TiO_2 nanoparticles fabricated by Ti-PIII have a size of about 20 nm, which is close to the favorable size for integrin clustering and focal contact formation of cells, thus providing step-by-step anchoring points for the bMSCs and maintaining good cell vitality. In addition to the TiO_2 nanoparticles, the large pores induce the effects to elongate/stretch cell bodies, which are considered to up-regulate osteoblastic expressions [26]. Hence, the nanopores with TiO_2 walls combine the advantages of both small and large TiO_2 nanotubes.

Other than bio-activating bMSCs, the nanopores with TiO_2 walls possess the ability to influence bacteria growth. It is known that interface between the implant surface and human tissues is vulnerable and can easily become the hotbed for bacteria growth which is gradually becoming one of main reasons for post-surgical implant failure [46]. Hence, it is imperative to design surfaces with intrinsic antibacterial properties. Here, according to the bacteria counting tests and SEM, the Ti-PIII modified surface can effectively reduce *S. aureus* adhesion and growth and also has a partially influence on *E. coli* (Figs. 9 and 10). According to ICP-AES (Table 4), there is no obvious release of Ti ions. Therefore, it appears that the main bacteria killing mechanism is physical contact. The Ti nanoparticles on the CFRPEEK surface undergo gradual oxidation upon exposure to air and transform into oxygen-vacant or oxygen-deficient titanium oxide. Oxygen vacancies in TiO_2 are highly reactive and reactive oxygen species (ROS) are produced in the microenvironment to damage the bacteria surface causing cell death [47,48]. Compared to bacteria, bMSCs are larger and have a more advanced metabolic system to resist the ROS. Our data disclose that *S. aureus* is more vulnerable than *E. coli* in this environment and it is believed to be due to the different shape of the two bacteria. Unlike the dissociative TiO_2 nanoparticles, the chances to directly contact TiO_2 nanoparticles on the structured substrate are much different for *S. aureus* and *E. coli*. Compared to *S. aureus* (round shape), *E. coli* has an elongated shape which may reduce direct contact with the TiO_2 nanoparticles and hence minimizing the influence of ROS.

Table 4
Ti ion concentration in PBS after immersion for different time.

Immersion time (days)	7	14	21	28
Ti ion concentration (μg/mL)	0.00487	0.0049	0.00501	0.00517

5. Conclusion

Energetic ion bombardment and surface micro-charging are utilized synergistically in Ti plasma immersion ion implantation top produce nanopores with TiO_2 walls on CFRPEEK. The multilevel nanoporous surface on CFRPEEK has improved elastic recovery and acceptable stability. Adhesion, proliferation, and osteoblastic differentiation of bMSCs on the nanoporous CFRPEEK surface are promoted. Moreover, partial resistance to *Staphylococcus aureus* and *Escherichia coli* is observed due to the unique multilevel nanoporous structure with TiO_2 nanoparticles. The surface properties of CFRPEEK are improved by this method and the application of plasma treated CFRPEEK to orthopedic and dental implants is expected to be broadened and expedited.

Acknowledgments

Joint financial support from the National Basic Research Program of China (973 Program, 2012CB933600), National Natural Science Foundation of China (81271704 and 31370962), Shanghai Science and Technology R&D Fund under grants 11JC1413700, Hong Kong Research Grants Council (RGC) General Research Funds (RGC) No. 112212, and City University of Hong Kong Applied Research Grants (ARG) No. 9667066 and 9667069 is acknowledged.

References

[1] Navarro M, Michiardi A, Castano O, Planell JA. Biomaterials in orthopaedics. J R Soc Interface 2008;5:1137–58.
[2] Kurtz SM, Devine JN. PEEK biomaterials in trauma, orthopedic, and spinal implants. Biomaterials 2007;28:4845–69.
[3] Sagomonyants KB, Jarman-Smith ML, Devine JN, Aronow MS, Gronowicz GA. The in vitro response of human osteoblasts to polyetheretherketone (PEEK) substrates compared to commercially pure titanium. Biomaterials 2008;29:1563–72.
[4] Wang HY, Xu M, Zhang W, Kwok DTK, Jiang JA, Wu ZW, et al. Mechanical and biological characteristics of diamond-like carbon coated poly aryl-ether-ether-ketone. Biomaterials 2010;31:8181–7.
[5] Abu Bakar MS, Cheng MHW, Tang SM, Yu SC, Liao K, Tan CT, et al. Tensile properties, tension-tension fatigue and biological response of polyetheretherketone-hydroxyapatite composites for load-bearing orthopedic implants. Biomaterials 2003;24:2245–50.
[6] Brockett CL, John G, Williams S, Jin Z, Isaac GH, Fisher J. Wear of ceramic-on-carbon fiber-reinforced poly-ether ether ketone hip replacements. J Biomed Mater Res B Appl Biomater 2012;100B:1459–65.
[7] Pei X, Friedrich K. Erosive wear properties of unidirectional carbon fiber reinforced PEEK composites. Tribol Int 2012;55:135–40.
[8] Toth JM, Wang M, Estes BT, Scifert JL, Seim HB, Turner AS. Polyetheretherketone as a biomaterial for spinal applications. Biomaterials 2006;27:324–34.
[9] Khonsari RH, Berthier P, Rouillon T, Perrin J-P, Corre P. Severe infectious complications after PEEK-derived implant placement: report of three cases. J Oral Maxillofac Surg Med Pathol; 2014. In Press, http://dx.doi.org/10.1016/j.ajoms.2013.04.006.
[10] Chu PK. Bioactivity of plasma implanted biomaterials. Nucl Instrum Methods Phys Res B 2006;242:1–7.
[11] Chu PK. Plasma surface treatment of artificial orthopedic and cardiovascular biomaterials. Surf Coat Technol 2007;201:5601–6.
[12] Chu PK. Recent applications of plasma-based ion implantation and deposition to microelectronic, nano-structured, and biomedical materials. Surf Coat Technol 2010;204:2853–63.
[13] Garcia JA, Rodriguez RJ. Ion implantation techniques for non-electronic applications. Vacuum 2011;85:1125–9.
[14] Wang J, Huang N, Pan CJ, Kwok SCH, Yang P, Leng YX, et al. Bacterial repellence from polyethylene terephthalate surface modified by acetylene plasma immersion ion implantation-deposition. Surf Coat Technol 2004;186:299–304.
[15] Cao H, Liu X, Meng F, Chu PK. Biological actions of silver nanoparticles embedded in titanium controlled by micro-galvanic effects. Biomaterials 2011;32:693–705.
[16] Qian S, Cao H, Liu X, Ding C. Nanotube array controlled carbon plasma deposition. Appl Phys Lett 2013;102:243109.
[17] Li XC, Wang YN. Effects of charging at dielectric surfaces on the characteristics of the sheath for plasma immersion ion implantation. Acta Phys Sin 2004;53:2666–9.
[18] Fu RKY, Tian X, Chu PK. Enhancement of implantation energy using a conducting grid in plasma immersion ion implantation of dielectric/polymeric materials. Rev Sci Instrum 2003;74:3697–700.
[19] Oates TWH, Bilek MMM. Insulator surface charging and dissipation during plasma immersion ion implantation using a thin conductive surface film. J Appl Phys 2002;92:2980–3.
[20] Dalby MJ, Gadegaard N, Tare R, Andar A, Riehle MO, Herzyk P, et al. The control of human mesenchymal cell differentiation using nanoscale symmetry and disorder. Nat Mater 2007;6:997–1003.
[21] Bennett CN, Longo KA, Wright WS, Suva LJ, Lane TF, Hankenson KD, et al. Regulation of osteoblastogenesis and bone mass by Wnt10b. Proc Natl Acad Sci U S A 2005;102:3324–9.
[22] Oh S, Brammer KS, Li YSJ, Teng D, Engler AJ, Chien S, et al. Stem cell fate dictated solely by altered nanotube dimension. Proc Natl Acad Sci U S A 2009;106:2130–5.
[23] Ciapetti G, Ambrosio L, Marletta G, Baldini N, Giunti A. Human bone marrow stromal cells: in vitro expansion and differentiation for bone engineering. Biomaterials 2006;27:6150–60.
[24] Neoh KG, Hu X, Zheng D, Kang ET. Balancing osteoblast functions and bacterial adhesion on functionalized titanium surfaces. Biomaterials 2012;33:2813–22.
[25] Puckett SD, Taylor E, Raimondo T, Webster TJ. The relationship between the nanostructure of titanium surfaces and bacterial attachment. Biomaterials 2010;31:706–13.
[26] Brammer KS, Oh S, Cobb CJ, Bjursten LM, van der Heyde H, Jin S. Improved bone-forming functionality on diameter-controlled TiO_2 nanotube surface. Acta Biomater 2009;5:3215–23.
[27] Park J, Bauer S, Schlegel KA, Neukam FW, von der Mark K, Schmuki P. TiO_2 nanotube surfaces: 15 nm-an optimal length scale of surface topography for cell adhesion and differentiation. Small 2009;5:666–71.
[28] Park J, Bauer S, von der Mark K, Schmuki P. Nanosize and vitality: TiO_2 nanotube diameter directs cell fate. Nano Lett 2007;7:1686–91.
[29] Huo K, Zhang X, Wang H, Zhao L, Liu X, Chu PK. Osteogenic activity and antibacterial effects on titanium surfaces modified with Zn-incorporated nanotube arrays. Biomaterials 2013;34:3467–78.
[30] Popat KC, Eltgroth M, La Tempa TJ, Grimes CA, Desai TA. Titania nanotubes: a novel platform for drug-eluting coatings for medical implants? Small 2007;3:1878–81.
[31] Ingo GM, Dire S, Babonneau F. XPS studies of SiO_2-TiO_2 powders prepared by sol-gel process. Appl Surf Sci 1993;70-1:230–4.
[32] Saied SO, Sullivan JL, Choudhury T, Pearce CG. A comparison of ion and fast atom beam reduction in TiO_2. Vacuum 1988;38:917–22.
[33] Liu XY, Poon RWY, Kwok SCH, Chu PK, Ding CX. Structure and properties of Ca-plasma-implanted titanium. Surf Coat Technol 2005;191:43–8.
[34] Liu XY, Zhao XB, Fu RKY, Ho JPY, Ding CX, Chu PK. Plasma-treated nanostructured TiO_2 surface supporting biomimetic growth of apatite. Biomaterials 2005;26:6143–50.
[35] Maitz MF, Poon RWY, Liu XY, Pham MT, Chu PK. Bioactivity of titanium following sodium plasma immersion ion implantation and deposition. Biomaterials 2005;26:5465–73.
[36] Poon RWY, Ho JPY, Liu XY, Chung CY, Chu PK, Yeung KWK, et al. Anti-corrosion performance of oxidized and oxygen plasma-implanted NiTi alloys. Mater Sci Eng A Struct Mater 2005;390:444–51.
[37] Liu X, Fu RKY, Ding C, Chu PK. Hydrogen plasma surface activation of silicon for biomedical applications. Biomol Eng 2007;24:113–7.
[38] Wang H, Kwok DTK, Wang W, Wu Z, Tong L, Zhang Y, et al. Osteoblast behavior on polytetrafluoroethylene modified by long pulse, high frequency oxygen plasma immersion ion implantation. Biomaterials 2010;31:413–9.
[39] Zhang W, Wang H, Oyane A, Tsurushima H, Chu PK. Osteoblast differentiation and disinfection induced by nitrogen plasma-treated surfaces. Biomed Mater Eng 2011;21:75–82.
[40] Anders A. Atomic scale heating in cathodic arc plasma deposition. Appl Phys Lett 2002;80:1100–2.
[41] Schneider GAA. Griffith type energy release rate model for dielectric breakdown under space charge limited conductivity. J Mech Phys Solids 2013;61:78–90.
[42] Hibma T, Zeller HR. Direct measurement of space-charge injection from a needle electrode into dielectrics. J Appl Phys 1986;59:1614–20.
[43] Powles RC, McKenzie DR, Meure SJ, Swain MV, James NL. Nanoindentation response of PEEK modified by mesh-assisted plasma immersion ion implantation. Surf Coat Technol 2007;201:7961–9.
[44] Albu SP, Ghicov A, Aldabergenova S, Drechsel P, LeClere D, Thompson GE, et al. Formation of double-walled TiO_2 nanotubes and robust anatase membranes. Adv Mater 2008;20:4135-+.
[45] Richert L, Vetrone F, Yi JH, Zalzal SF, Wuest JD, Rosei F, et al. Surface nanopatterning to control cell growth. Adv Mater 2008;20:1488-+.
[46] del Pozo JL, Patel R. The challenge of treating biofilm-associated bacterial infection. Clin Pharmacol Ther 2007;82:204–9.
[47] Adams LK, Lyon DY, Alvarez PJJ. Comparative eco-toxicity of nanoscale TiO_2, SiO_2, and ZnO water suspensions. Water Res 2006;40:3527–32.
[48] Heinlaan M, Ivask A, Blinova I, Dubourguier HC, Kahru A. Toxicity of nanosized and bulk ZnO, CuO and TiO_2 to bacteria Vibrio fischeri and crustaceans Daphnia magna and Thamnocephalus platyurus. Chemosphere 2008;71:1308–16.